XIV International Conference on Computational Plasticity. Fundamentals and Applications
COMPLAS 2019
E. Oñate, D.R.J. Owen, D. Peric , M. Chiumenti, and Eduardo de Souza Neto (Eds)

CALCULATION OF SUB-SURFACE-INITIATED FATIGUE FRACTURES IN GEARS

DANIEL MÜLLER, THOMAS TOBIE AND KARSTEN STAHL

Gear Research Centre (FZG)
Technical University of Munich (TUM), Germany
email: fzg@fzg.mw.tum.de, website: http://www.fzg.mw.tum.de

Key words: Residual Stresses, Tooth Flank Fracture, Load Carrying Capacity, Gears

Abstract. Power-transmitting gears are typically heat-treated, most often case-hardened, to improve the fatigue strength and therefore to ensure higher fatigue life. The heat treatment causes higher hardness in the surface area as well as compressive residual stresses in the hardened layer. The near-surface compressive residual stresses are compensated by tensile stresses in higher depths of the gear volume.
Pitting and tooth root breakage are the most common failure modes of gears, which are well researched and are also addressed in ISO 6336 [14]. The assessment of these failure modes provides the basis for the dimensioning of gears in the design phase. However, subsurface-initiated failures, like tooth flank fracture (TFF), can also appear at loads below the allowable level of loading for pitting and tooth root bending. TFF is a fatigue damage with crack initiation in the region of the transition between compressive and tensile residual stresses and usually leads to a total loss of drive.

The existing calculation models for fatigue strength of gears with regard to TFF consider residual stresses differently. The base of the investigated calculation models is a local comparison of the occurring stresses and the strength value in the gear volume. The outcome of the calculation model from Oster [26] is highly influenced by the residual stress state. However, the material-physical model by Hertter [10] is more tolerant to slightly varying residual stresses. Further approaches such as Weber [34] and Konowalcyk [18] are based on the ideas of Oster and Hertter.

The verification of the models is complicated due to the lack of residual stress measurements in larger depths under the gear flank surface. For example, residual stress measurement by X-ray diffraction is only possible up to depths of approximately one millimeter. Therefore, tensile residual stresses in the inner tooth volume are considered zero in the common residual stresses calculation of Lang [19] and are not considered in the current calculation approach of ISO/DTS 6336-4 [15].

The paper describes local calculation approaches for the fatigue strength of gears with different consideration of residual stresses. Furthermore, the crack initiation point, which is mandatory for the validation of an approach, is examined. The failure mode TFF is hereby the key.

1 INTRODUCTION

Power-transmitting gears are loaded with a torque that results in contact pressure at the transmitting tooth flanks. These gears are usually heat-treated to achieve higher strength in the surface area. A common heat treatment is case hardening. Case hardening causes higher carbon content in the surface area and a change in the microstructure. The change in the microstructure causes higher hardness and additionally compressive residual stresses in the surface layer, which also support the strength of the gear [9]. The depth of the microstructure change is mostly dependent on the time the gear is heated. For gears, the case hardening process is described with the case hardening depth (CHD), which is the depth of a hardness of 550 HV.

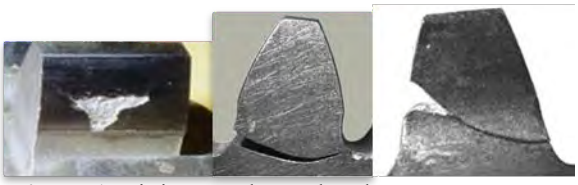

Figure 1: Pitting, tooth root breakage, TFF

To achieve a specified lifetime, different failure modes need to be prevented. The classical failure modes are pitting, tooth root breakage, micropitting, scuffing and wear. The main fatigue failure risks of a gear are currently pitting and tooth root breakage (**Figure 1**). Both failures are initiated by cracks in the near surface area due to cyclic loading. The calculation of the load capacity of these failure modes is well researched and very well manageable with ISO standards (ISO 6336 [14]). In recent years, subsurface-initiated failures have increased due the practice of higher loading and higher material strength at the surface. In addition, the adjustment of the residual stress state in the surface area lead to higher load capacities, which shifted the possible crack initiation in higher depths of the gear. Subsurface-initiated failures are for example tooth flank fracture (TFF).

2 DEFINITION OF TOOTH FLANK FRACTURE (TFF)

Subsurface-initiated failures have the crack initiation point (PR) in higher depths where the material strength of the heat-treated gear declines and significantly lower stresses than at the near surface can lead to crack initiation and growth with every loading cycle. The characteristics of the tooth flank fracture are described in various papers and dissertations [4, 7, 8, 36]. This paper describes tooth flank fracture for case-hardened external spur and helical gears. However, there are TFFs also reported for bevel and hypoid gears but not discussed in this paper [1, 6].

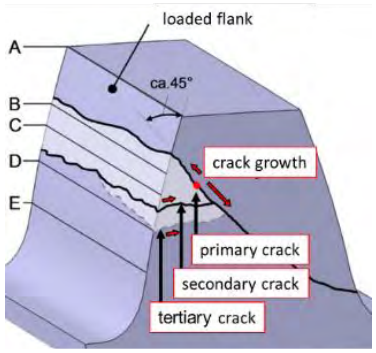

Figure 2: TFF crack growth [4]

TFF is a high cycle fatigue failure. The failure shows S-N curve behavior and therefore the characteristics of a limited lifetime at high loads and an endurance limit at lower loads. The crack growth is slower towards the surface due to the higher material strength. Therefore, the crack is growing internally and is not visible until breakage. The crack initiation is located in the area between the surface and core hardness and mostly where the hardness reaches the core hardness. In addition to the primary crack, secondary and tertiary cracks can occur [36]. The crack growth is internal and slow and under vacuum; therefore, a fisheye around the crack imitation is possible but not mandatory [3]. Due to varying loading, beachmarks indicating the crack growth are possibly visible in the fisheye as shown in

Figure 3. The crack often starts at an inclusion or irregularities in the micro-structure due to a possible local stress increase. [36]

The main influences are the material strength profile , the contact stresses and the residual stresses in higher depths. Additional stresses due to the deformation of the tooth are considered as less significant and depend on the geometry of the tooth [8, 36],30].

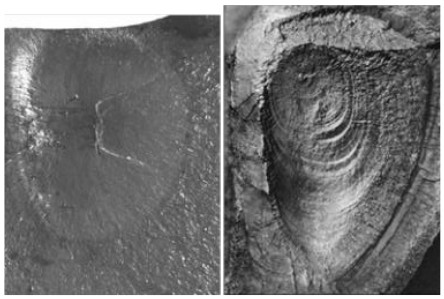

Figure 3: Characteristics of tooth flank fracture, fisheye of constant loading [7], fisheye with beachmarksdue to the crack growth under varying loading [1]

Experimental results of test gears are described in the works of Tobie [33], Bruckmeier [8] and Witzig [36]. Witzig did substantial experimental research. Different gear geometries with different materials were tested with varying loading conditions up to 100 million load cycles in an FZG back-to-back test rig. The gear set with module 3 mm and 67/69 teeth of these experimental investigations is possibly the most discussed for the evaluation of TFF calculation approaches. TFF is observed in a range of 1 million up to 100 million load cycles for this gear geometry. In addition, a calculation approach is presented in Witzig based on the Superior FZG-Modell. Nevertheless, this failure mode is still much less researched compared to other failures such as pitting and tooth root breakage.

3 STRESS CALCULATION

While transmitting torque, a single tooth of the gear is loaded with different stresses, which are responsible for a possible occurring failure mode. For subsurface-initiated failure modes, the super-positioning of several loading stresses is possibly relevant.

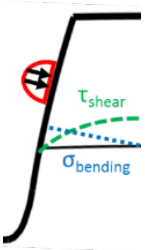

Figure 4: Tooth shear stresses and bending stresses

The main stresses due to loading are the contact stresses after Hertzian theory. Stresses due to the shear of the tooth and bending of the tooth strongly depend on the geometry of the gear set [8, 36]. The stresses due to tooth shear load are maximal in the middle of the tooth and constantly distributed in the tooth height under the contact point. Bending stresses with a maximum at the surface and near zero in the middle of the tooth decrease with increasing tooth height. The mentioned stresses have significantly different distributions as shown in **Figure 4**.

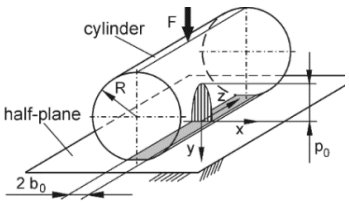

Figure 5: Theory of Hertz

The contact stresses of the rolling and sliding contact between the tooth flanks are described by the Hertzian theory [12]. The stresses depend on the loading of the flank, the local normal radius of relative curvature, the reduced modulus of elasticity and the tooth width of the pinion and the wheel. The loading and the radius of relative curvature depend on the contact point at the transverse path of contact. The normal contact force depends on the number of teeth in contact. Between point B and D, a maximum level of the normal force due the singular contact is reached. The radius of relative curvature is usually increasing until contact point D. This leads to a maximum contact stress

between the contact points B and D.

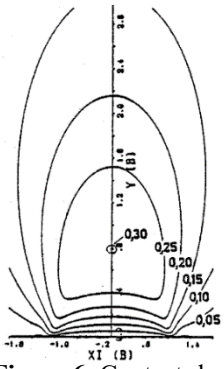

Figure 6: Contact shear stress with maxima [18]

The contact stresses after Hertz are described by the pressure p_H on the contact width $2\times b_H$ and based on a half space approach, where the two radii are combined to a relative radius of curvature, which is forced on a half plane. The elliptical distribution of pressure over the contact width $2\times b_H$ is constant over the contact length or respectively the tooth width. According to the Hertzian theory, the normal stresses are maximal at the surface and the shear stress maximum of $0.3\times p_H$ is at a depth of approximately $0.8\times b_H$ (**Figure 6**). The dependency of p_H on the radius of relative curvature means, that for gears with greater radius of curvature (such as large gears) the maximum shear stress is at a greater depth normal to the flank. These contact stresses can be calculated with the equations of Hertz or by the equations of Johnson [16] dependent on the Hertzian stress p_H and the half contact width b_H.

4 MATERIAL STRENGTH AND CALCULATION OF HARDNESS PROFILES

For the calculation of the material exposure, mostly local approaches are used. The local approach is a comparison of the local stress and the local material strength. The material strength is mostly derived from the hardness profile. Additionally, in some local calculation approaches, the yield strength R_p, tensile strength R_m or other strength parameters such as the alternating strength σ_w are used. These material-dependent parameters are gained by testing specimens under a defined load.

Different calculation approaches for the hardness profile are used in the design phase. The calculation is based on the CHD, the surface hardness and the core hardness, which are usually specified in the design phase. There are different approaches for the hardness profile for different heat treatment processes. In **Figure 7**, approaches for case hardening are compared to a representative measurement of the module 3 mm gear researched in Witzig [36].

The hardness of the material can be calculated with the equations after Lang [19], which is the most common approach. The approach of Lang is suitable for case hardening, induction hardening and nitriding. It requires the CHD, the surface hardness and the core hardness. For the tooth flank hardness profile, the core hardness measured at the flank area should be used for a better alignment with the measured hardness. Another approach for case-hardened gears is proposed by FZG/Thomas [32]. This approach has the ability to represent the hardness plateau in the near surface area, which occurs in large gears due to the case-hardening process. The plateau is calculated by the specification of the maximum hardness depth. Mack Aldner and Olsson proposed a hardness profile calculation [24]. For the approach, the carburization depth in addition to the surface hardness and core hardness is required. Beermann [5] proposed two alternatives for the approach of Lang. The two alternatives (A1 and A2) are mathematical corrections of the Lang equations, where the CHD is positioned at 550 HV.

Figure 7 shows a comparison of the mentioned hardness profile calculation approaches for a surface hardness of 700 HV1 and a core hardness of 440 HV1 with a CHD of 0.5 mm. By all approaches, the hardness measurement is described quite well under the consideration of the uncertainty of hardness measurements. The maximum hardness in the approach of Thomas is

assumed to be 0.0 and 0.08 mm to show the behavior of the approach. Differences in the approaches only exist in the transition to the core hardness, which is the critical area for TFF. For different gears and gear sizes, different approaches can be suitable. Due to the high influence on the material exposure in some existing calculation approaches for TFF, an exact calculation of the hardness profile is mandatory.

5 RESIDUAL STRESSES AND CALCULATION OF RESIDUAL STRESSES

Lang [19] also proposed an approach to calculate the residual stress profile (**Figure 7**). The calculation is only depending on the hardness profile. Improvements of the equations were made by FZG [8, 11] to adjust the residual stress in the surface area when the difference between the hardness profile and the core hardness is higher than 300 HV.

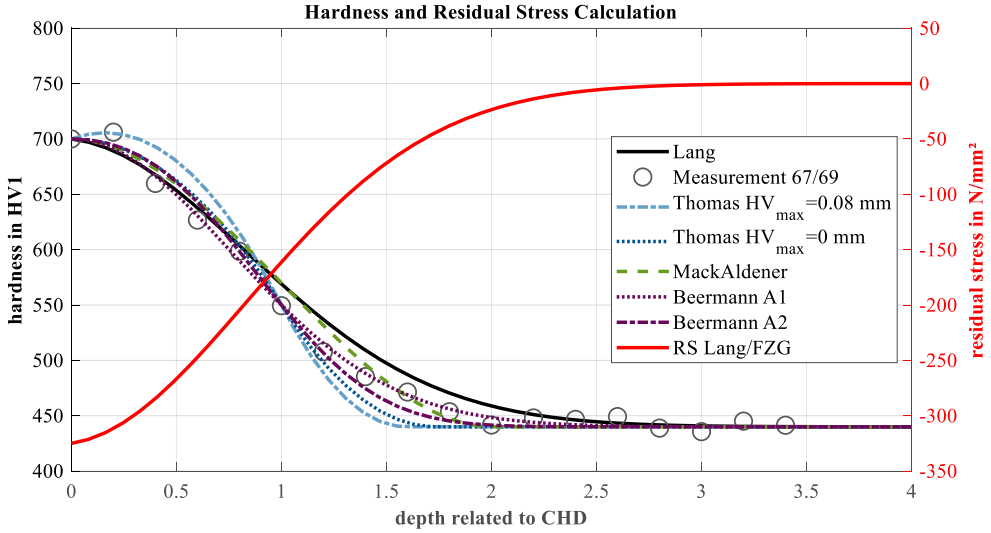

Figure 7: Hardness and residual stress calculation of different approaches compared to hardness measurement

The residual stresses are caused due the transformation of the micro-structure due to the heat treatment. They can be defined as three different kinds after the influenced area [23] . The total residual stress state is a superposition of all three kinds. The residual stresses are self-equilibrating stresses, which means there cannot be a resulting force or moment in the gear. Due to the mechanical equilibrium, compressive residual stresses must be compensated by tensile residual stresses. The calculation of Lang does not consider the tensile residual stresses, which should exist in higher depths of the tooth volume. In addition, the three-dimensional stress state is not considered.

A calculation approach with consideration of the tensile stresses is difficult to prove due to the complicated measurement of the residual stresses at higher depths. Still, calculation approaches with consideration of tensile residual stress are proposed. Konowalczyk [17] and Weber [34] proposed a similar approach. They append a polynomic function to the Lang approach at a depth of 0.5×CHD. The polynomic function is calculated by specified constraints with an algorithm to assure the mechanical equilibrium within the tooth thickness. These two approaches have the disadvantage of using an algorithm that can lead to no result and is difficult for the use in a standard calculation method such as ISO standard. In addition, a small tooth thickness can lead

to a high overestimation of the residual stresses especially in the near tooth addendum area. Furthermore, the three-dimensional stress state is not considered and an equilibrium of the hoop stresses is assumed.

For the validation of the residual stress state, measurements at great depths are necessary. Usually the tangential and axial residual stresses are measured with X-ray diffraction. The X-ray diffraction is applied at the surface of the specimen. By stepwise electrochemical polishing and measuring, a depth profile is gained [29]. The reachable depth is limited by the evenness of the bottom of the crater. Typically, depths up to 1 mm are usually possible. Measurements of greater depths are possible with neutron diffraction. In [27,36], measurements of two different tooth geometries are shown. The measurement results of the module 3 mm gear, which is prone to TFF are shown in **Figure 8**. The measurements at FRM II support the assumptions of Witzig et al. [36,34,20] that in larger material depth the residual stresses in normal (hoop) direction to the flank surface are near zero and the axial and radial stresses show no significant difference with consideration of the error.

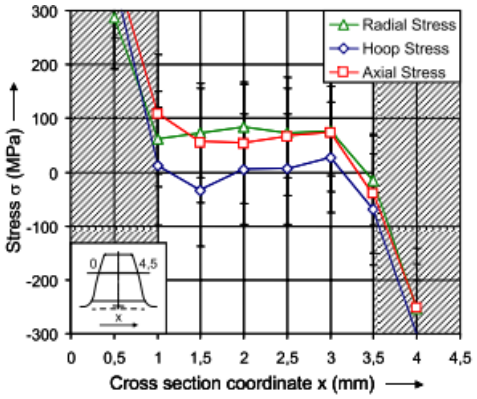

Figure 8: Residual stress measurment of the module 3 gear with neutron diffraction [24]

6 CALCULATION APPROACHES FOR TFF

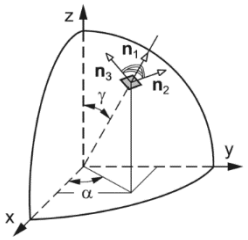

Figure 10: A quarter of sphere with coordinate system [15]

The calculation of subsurface-initiated fractures is based on a comparison of the local stress and local material strength. The quotient is defined as a local material exposure A. The local material strength is described by one-dimensional parameters as described earlier. For material strength, only one-dimensional data is generated e.g. tensile strength by tensile testing. The comparison to a three-dimensional stress state is possible with a multiaxial fatigue criterion.

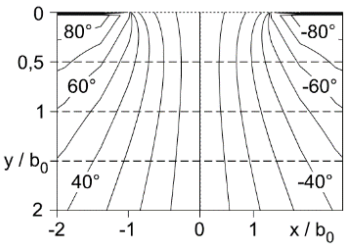

Figure 9: Principal stress direction in rolling and sliding

The loading of the part results in stresses at the planes of the infinite small spherical element. Due to the equilibrium of moment, the shear stresses are the same over the diagonal (symmetry). For the calculation of the stresses in a specific direction a transformation is applied. The direction can be described by a plane at the surface of a sphere, which is described by two angels (α, γ) as shown in **Figure 10**. At specific angles, the stress vector is normal to the plane and the shear stresses are zero. These directions are called principle stress directions. By calculation invariants of the stress tensor, a description of the stress state independent from the body coordinate system is gained. The second invariant is used in the von Mises criterion for the description of failures. It also allows the separation of the hydrostatic stresses and the deviatoric stresses.
The subsurface contact stresses change due to the loading rolling and sliding contact. Also, the principal stress coordinate changes as shown in **Figure 9**. A volume element in a specific depth therefore has a time-dependent stress tensor.

The path of the stresses is described in the planes of the infinite small spheres. The shear stresses change in the direction of the plane and normal stresses change normal to the plane.

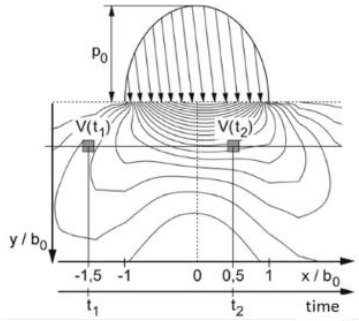

Figure 11: Stress on volume element in the contact area [11].

The stresses in the planes described by alpha and gamma are the basis of the following explanations. The hypotheses can then be divided into hypotheses of the critical plane and integral hypotheses. The critical plane approaches only take the plane with maximum stress into account and ignore the orientation of the micro-structure and assume that the maximum stress is occurring in a slip plane of the micro-structure. The crack initiation is caused by a shear stress high enough to cause plastic deformation when a slip plane is hit. The integral methods regard stresses in all planes.

The shear stress intensity hypothesis (SIH) is an integral criterion. It is based on the interpretation of the von Mises criterion of Novožilov [25] and can be derived from the weakest link theory of Weibull [22, 35]. The SIH is suitable for changing principal stress directions. This criterion satisfies the demands of invariance of the coordinate system on the body and the principal stress coordinate system because all planes are taken into account. [37, 38]. Also after Liu [21] and the SIH after Zenner [38] are the most suitable for the endurance limit of multiaxial stresses with differences in frequency, phase or arbitrarily oscillating loads. The SIH is based on the von Mises criterion. The distortion energy theory (GEH) and shear stress theory (SH) are included when the directions of the principle stresses are constant. The SIH has different forms: the SIH after Simbürger [28] where the failure criterion is the quadratic mean of the material exposure in all planes and after Zenner [38] where the quadratic mean of the effective shear stresses lead to the equivalent stress. The effective shear stress is also used in the SIH variant used by Oster. The SIH used by Hertter for the calculation of the maximum exposure is based on Liu and Zenner. The treatment of residual stresses in these multiaxial criteria is not discussed yet because the influence of residual stresses is usually considered as mean stresses in the material strength.

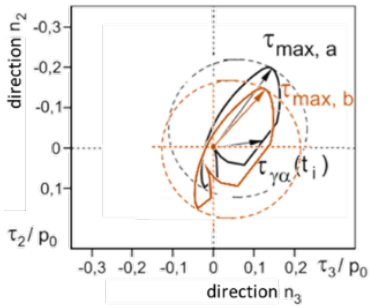

Figure 12: Shear stress path in a plane. a: without compressive residual stress; b: with compressive residual stress [Her03]

For TFF calculation where the residual stresses considered the second highest impact after contact stresses also approaches exist with a superposition of the residual stress state and the loading stress state after the application of a multiaxial stress hypothesis. One of these approaches is after FZG/Oster which results in a good TFF prediction [7]. For TFF prediction with a local approach, the following requirements need to be fulfilled: the height of the calculated material exposure predicts TFF. Thereby the calculated local maximum exposure is at the experimental observed depth of PR and position on the contact path respectively tooth height. Additionally, the calculated material exposure correlates with load cycles in a limited lifetime.

A calculation approach for surface failure and subsurface failure is stated in Oster [26]. Oster describes the shear stress intensity as the quadratic mean value of the maximum shear stress in

all planes which corresponds to the procedure in [38].

$$\tau_{eff} = \sqrt{\frac{1}{4\pi}\int_{\gamma=0}^{\pi}\int_{\alpha=0}^{2\pi}\tau_{\gamma\alpha,max}^{2}\sin\gamma\, d\alpha\, d\gamma} \tag{1}$$

The maximum shear stress in the planes is composed of the normal contact stresses, the shear contact stresses due to friction, the thermal stresses and the residual stresses. The path of the shear stresses in a plane consist of the transition of the Hertzian pressure as shown in **Figure 11**. The effective stress state of the residual stresses is subtracted from the overall effective stress state. The local material exposure A is the quotient of the effective stress state and the allowable shear stress. (2)

$$\tau_{eff\,DA} = \tau_{eff\,Load,RS} - \tau_{eff\,RS}$$

The allowable shear stress is derived from the hardness profile. The constant of proportionality k is approximately 0.4 and further specified for different materials and tooth geometries in [36].

$$\tau_{zul}(y) = k \cdot HV(y) \tag{3}$$

The approach of FZG/Hertter [11] is an extended approach of the approach after FZG/Oster. Hertter separates the dynamic exposure A_{int_a}, which considers the amplitude and mean values of stress and a maximum exposure A_{int} considering the maximum shear and normal stress. Results of calculations show that the maximum material exposure for the evaluation of gears in higher component depths is decisive. The exposure A is calculated in all planes with equation after Liu [21]. The residual stresses are considered in the maximum shear and maximum normal stresses in all planes as shown in in **Figure 12**.

$$A_{max}(\gamma,\alpha) = \sqrt[\mu]{\frac{a\cdot\tau_{max}^{\mu} + b\cdot\sigma_{max}^{\mu}}{R_{p0,2}^{\mu}}} \tag{4}$$

The allowable stress is defined by the yield strength, which is derived from the local hardness after [13]. The local material exposure is calculated by the integration of the exposure in all planes.

$$A_{int} = \sqrt{\frac{15}{8\pi} * \int_{\gamma=0}^{\pi}\int_{\alpha=0}^{2\pi}[A_{max}(\gamma,\alpha)]^2 * \sin\gamma\, d\alpha\, d\gamma} \tag{5}$$

7 INVESTIGATIONS ON THE CRACK INITIATION POINT OF TFF

For the validation of the different calculation approaches, the primary crack starter depth and the corresponding load or the endurance limit need to be investigated for different gears and materials. Due the different depths of maximum stress of the contact, bending and tooth shear stresses, the primary crack initiating point (PR) also gives a hint of which stress is more or less responsible for TFF. In this section, the PR of TFF is further investigated; therefore, the TFF reference gear set with module 3 mm and 67/69 teeth is examined.

Tobie [33] was the first to investigate TFF at the FZG back-to-back test rig for the gear set. The gears were made out of the material 16MnCr5 with an CHD of 0.55 mm. In Stenico [31], the

gear geometry was investigated referring to inclusions in the material. Bruckmeier [8] did test runs with gears of the material 16MnCr5 and 17CrNiMo6. The gears were also case-hardened with a CHD of 0.5-0.55 mm. With the experiments of Witzig [36], the first S-N curves for TFF were completed. He investigated the case-hardened materials 18CrNiMo7-6 and 20MnCr5 with a CHD of ca. 0.5 mm. The endurance limit for 18CrNiMo7-6 was 1460 Nm and for 20MnCr5 1250 Nm. The hardness profile of the gears is comparable with a surface hardness of 690-785 HV and core hardness of 364-440 HV.

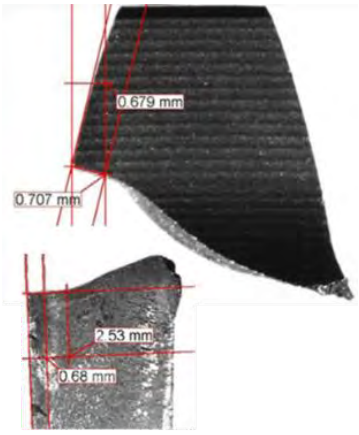

Figure 13: Optical-digital measurement of the PR.

All mentioned authors did research on the PR. The PR is usually identified visually. When observing the fracture surface, a microscope or scanning electron microscope (SEM) can help find the PR. The crack surface usually shows the characteristics of a fatigue fracture with a smooth surface in the area of ductile breakage and a rough surface where the final rupture is. Usually a fisheye is visible in the area of ductile breakage. The PR is usually placed central in the fisheye. For some TFF, a PR is not necessarily detectable.

For this paper, the PRs for the 67/69 gear with module 3 mm and a pressure angle of 20° of these works were summarized and further investigated. The authors [8, 33, 36] measured the PR optical with a digital photo station. For some teeth, the PR was investigated by scanning with an electron microscope with EDX to gain information of a possible nonmetallic inclusion in the material [36]. The depth of the PR was specified in the direction normal to the tooth flank.

The crack initiation points of TFF were further investigated to find the correlation of the PR depth with loading or heat treatment parameters. The residual stress measurements with X-ray diffraction were only up to a depth of 0.32 mm. The investigated PR depth is higher and therefore residual stresses are not considered in the evaluation.
Additional teeth of Witzig were measured digital with a digital photo station. First, the PR was identified by its characteristics. Then photos of the sides of the tooth are taken to digitally measure the exact position normal to the flank as shown in **Figure 13**. The error of the measurement is approximately 0.1 percent due the constraints of the digital photo station and the angle error due to the placement of the teeth in the digital photo station.

For the results, a correlation between PR depth and load or load cycles is not observed. But a dependency on the load is expected when the contact stresses are a main influence. Due to higher loading the maximum contact shear stresses are in greater depths normal to the flank after the theory of Hertz. For correlation with loading parameters (such as the torque), a separation of materials is not necessary because the depth of maximum exposure depends on the contact stresses and the hardness which is comparable. This supports a statement of Konowalczyk [17], who also observed no correlation between loading and the PR depth.

A good correlation of PR depth and the CHD was found as shown in **Figure 14**. The assumption of a normal distribution is possible with a mean of 2.57×CHD (1.29 mm) and standard deviation of 0.68×CHD. Other gear geometries show PRs at higher depths (up to 3.6×CHD in Stenico [31]) or at smaller depths 1-1.5×CHD [2].

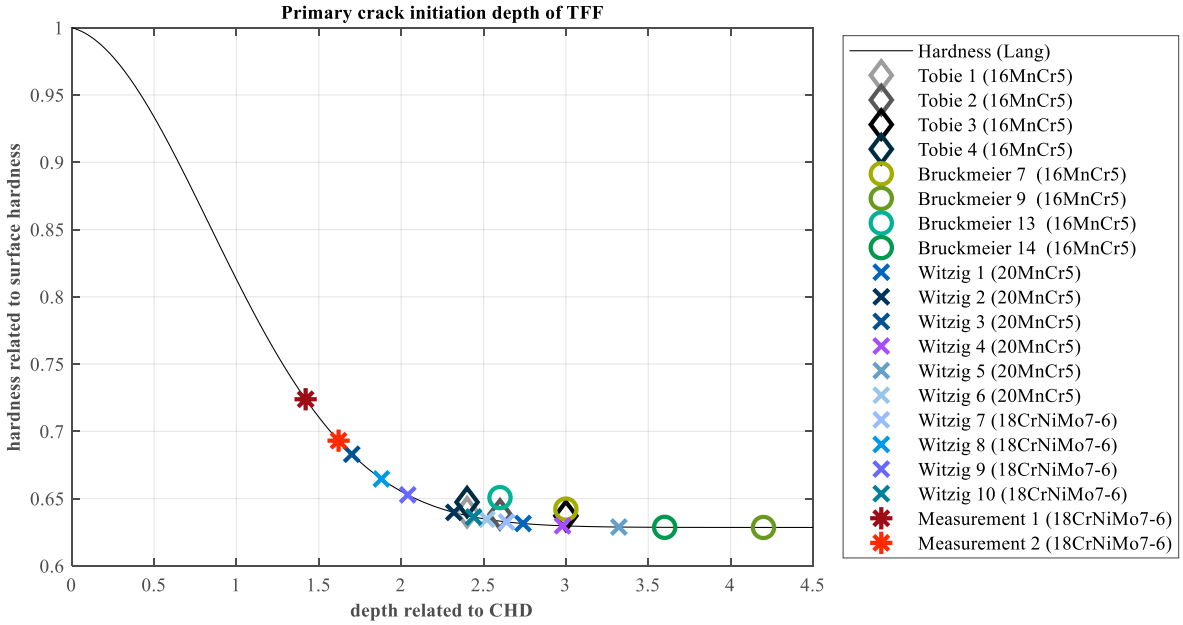

Figure 14: Crack initiation depth of TFF for the module 3 mm 67/69 teeth gear set.

8 CONCLUSIONS

For higher strength in gears, a heat treatment like case hardening is used. Case hardening improves the surface strength due to higher hardness and compressive residual stresses in the surface area. The mechanically required tensile residual stresses in the inner tooth are considered promoting crack initiation and crack growth. TFF is a subsurface-initiated fracture with a primary crack starter in depths of reduced strength. The PR is located deeper than the maximum shear stress after the theory of Hertz and therefore residual stresses are considered a main influence on the crack initiation.

For TFF, several calculation approaches are proposed, which treat the residual stresses differently. For the validation of a local TFF calculation approach, the local residual stress state is required and for the validation the crack initiation point of TFF and the corresponding load are mandatory. This paper summarizes the documented crack initiation depth of the module 3 mm gear set with 67/69 teeth. Also, additional TFFs of this geometry are analyzed and measured by optical-digital measurement. The crack initiation depth is further investigated and correlations with the CHD are shown. However, no correlation with load parameters is found.

More primary crack initiation points of different gear geometries need to be investigated and documented with geometry, load and heat treatment parameters for a statistically verified statement. For the validation of the calculation approaches, further investigations of the three-dimensional residual stress state in the inner tooth and its handling in the multiaxial criteria or the strength within the mean stresses are necessary. For an evaluation of the influence on the crack behavior of TFF in the multiaxial fatigue criteria, it is necessary to exclude additional influences of the microstructure such as carbon content and retained austenite content. Therefore, in Stahl [29], blanked representative parts are manufactured with adjustable residual stress state and without heat treatment. The application of the multiaxial criteria on these parts

will provide a further understanding of the treatment of residual stresses in the subsurface fracture calculation of gears.

ACKNOWLEDGEMENTS

Part of this work is funded by the Deutsche Forschungsgemeinschaft (DFG, German Research Foundation) - VO 1487/30-1; STA 1198/13-1 and is part of the DFG priority program “Targeted Use of Forming Induced Residual Stresses in Metal Components (SPP2013).”

REFERENCES

[1] Annast, R.: Kegelrad-Flankenbruch. Dissertation, Technische Universität München (2003).
[2] Bauer, E.: Flankenbrüche bei Hochleistungsgetrieben Allianz Report 2/98 (1998).
[3] Bauer, E.; Böhl, A.: Flank Breakage on Gears for Energy Systems. Gear Technology 28. Heft: 8, S. 36–42 (2011).
[4] Baydu Al; Langlois, P.: Evaluation of TIFF and TFF Load Carrying Capacities and Comparison Against Other Failure Modes. CTI MAG (2016).
[5] Beermann, S.: Tooth Flank Fracture - Influence of Macro and Micro Geometry. International Conference on Gears, Garching. VDI (2015).
[6] Boiadjiev, I.; Stemplinger, J.-P.; Stahl, K.: New Method for Calculation of the Load Carrying Capacity of Bevel and Hypoid Gears regarding Tooth Flank Fracture. Conference on Gears, Garching (2015).
[7] Boiadjiev, I.; Witzig, J.; Tobie, T.; Stahl, K.: Tooth flank fracture - basic principles and calculation model for a sub surface initiated fatigue failure mode of case hardened gears. International Conference on Gears, Lyon Villeurbanne, France, S. 670–80 (2014).
[8] Bruckmeier, S.: Flankenbruch bei Stirnradgetrieben. Dissertation, Technische Universität München (2006).
[9] Güntner, C.; Tobie, T.; Stahl, K.: Influences of the Residual Stress Condition on the Load Carrying Capacity of Case Hardened Gears Hardened Gears. AGMA (2017).
[10] Hertter, T.: A Calculation Model for Rating the Gear Load Capacity Based on Local Stresses and Local Properties of the Gear Material. International Conference on Gears; 2010; Garching (2010).
[11] Hertter, T.: Rechnerischer Festigkeitsnachweis der Ermüdungstragfähigkeit vergüteter und einsatzgehärteter Stirnräder. Dissertation, Technische Universität München (2003).
[12] Hertz, H.: Über die Berührung fester elastischer Körper (1881).
[13] Ilg, U.: Strukturelle Änderungen in unterschiedlich wärmebehandelten Wälzkörpern aus 100Cr6 und 20MnCr5 bei Wälz- sowie Wälz-Gleitbeanspruchung. Dissertation, Universität Karlsruhe (TH) (1980).
[14] ISO 6336, 2006,2016: Calculation of load capacity of spur and helical gears. (2006,2016).
[15] ISO/DTS 6336-4, 2018: Calculation of load capacity of spur and helical gears - Calculation of tooth flank fracture load capacity (2018).
[16] Johnson, K. L.: Contact mechanics. Cambridge University Press, Cambridge Cambridgeshire, New York, Port Melbourne, Madrid, Cape Town (1985).
[17] Konowalczyk, P.: Grübchen- und Zahnflankenbruchtragfähigkeit großmoduliger Stirnräder - Pitting and tooth flank fracture load capacity of large modul spur gears. Apprimus Verlag, Aachen (2018).
[18] Konowalczyk, P.; Löpenhaus, C.; Brecher, C.: Inclusion Based Calculation Approach for Flank Fracture Load Capacity. 58th Conference "Gear and Transmission Research" of the WZL on May 10/11 (2017).

[19] Lang, O. R.: Berechnung und Auslegung induktiv randschichtgehärteter Bauteile - In: Grosch, J.(Hrsg.), Induktives Randschichthärten, Tagung 23, S. 332-348. (1988).
[20] Liu, H.; Liu, H.; Zhu, C.; He, H.; Wei, P.: Evaluation of Contact Fatigue Life of a Wind Turbine Gear Pair Considering Residual Stress. Journal of Tribology 140-4 (2018).
[21] Liu, J.: Beitrag zur Verbesserung der Dauerfestigkeitsberechnung bei mehrachsiger Beanspruchung. Dissertation, TU Clausthal (1991).
[22] Liu, J.: Weakest Link Theory And Multiaxial Criteria 25, S. 55–68 (1997).
[23] Macherauch, E.: Introduction to Residual Stress. Advances in surface treatments, vol. 4. (1987).
[24] MackAldener, M.; Olsson, M.: Tooth Interior Fatigue Fracture - computational and material aspects. International Journal of Fatigue 23. Heft: 23 // 4, S. 329–40 (2001).
[25] Novožilov, V. V.: Theory of elasticity, Oxford (u.a.), Pergamon Pr., 1961 (1961).
[26] Oster, P.: Beanspruchung der Zahnflanken unter Bedingungen der Elastohydrodynamik. Dissertation, Technische Universität München (1982).
[27] Schwienbacher, S.; Tobie, T.; Höhn, B.-R.; Hofmann, M.: Measurement of Residual Stresses in Case Hardened Test Gears with Neutron-Diffractometer, Proposal No. 397 (2006).
[28] Simbürger, A.: Festigkeitsverhalten zäher Werkstoffe bei einer mehrachsigen, phasenverschobenen Schwingbeanspruchung mit körperfesten und veränderlichen Hauptspannungseinrichtungen. Dissertation, TH Darmstadt (1975).
[29] Stahl, J.; Müller, D.; Tobie, T.; Golle, R.; Volk, W.; Stahl, K.: Residual stresses in parts manufactured by near-net-shape-blanking. Production Engineering 23. Heft: 3, S. 217 (2018).
[30] Stahl, K.; Höhn, B.-R.; Tobie, T.: Tooth flank breakage - influences on subsurface initiated fatigue failures of case hardened gears. DETC2013, Portland, Oregon, USA. ASME (2013).
[31] Stenico, A.: Einfluss von Einschlüssen im Werkstoffgefüge auf den Beanspruchungszustand und das Schadensverhalten einsatzgehärteter Zahnflanken (2001).
[32] Thomas, J.: Flankentragfähigkeit und Laufverhalten von hart-feinbearbeiteten Kegelrädern. Dissertation, Technische Universität München (1998).
[33] Tobie, T.: Zur Grübchen- und Zahnfußtragfähigkeit einsatzgehärteter Zahnräder - Einflüsse aus Einsatzhärtungstiefe, Wärmebehandlung und Fertigung bei unterschiedlicher Baugröße. Dissertation, TU München (2001).
[34] Weber, R.: Auslegungskonzept gegen Volumenversagen bei einsatzgehärteten Stirnrädern. Dissertation, Universität Kassel (2015).
[35] Weibull, W.: A Statistical Theory of Strength of Materials (1939).
[36] Witzig, J.: Flankenbruch - Eine Grenze der Zahnradtragfähigkeit in der Werkstofftiefe. Dissertation, Technische Universität München (2012).
[37] Zenner, H.; Heidenreich, R.: Schubspannungsintensitätshypothese - Erweiterung und experimentelle Abstützung einer neuen Festigkeitshypothese für schwingende Beanspruchung (1979).
[38] Zenner, H.; Richter, I.: Festigkeitshypothese für die Dauerfestigkeit bei beliebigen Beanspruchungskombinationen. Konstruktion 29-1, S. 11–18 (1977).